DALTON
FULL PAPER

Synthesis and structural characterization of some tetraosmium carbonyl clusters incorporating pyridyl type ligands; mass spectrometric studies of the water soluble cationic tetraosmium carbonyl cluster $[Os_4(\mu\text{-}H)_4(CO)_{10}(dppH)]^+$ [dpp = 2,3-bis-(2-pyridyl)pyrazine] by electrospray techniques

Ya-Yin Choi and Wing-Tak Wong *

Department of Chemistry, The University of Hong Kong, Pokfulam Road, Hong Kong, P.R. China. E-mail: wtwong@hkucc.hku.hk

Received 20th October 1998, Accepted 2nd December 1998

The reactions of the activated tetraosmium carbonyl cluster $[Os_4(\mu\text{-}H)_4(CO)_{10}(NCMe)_2]$ **1** with some pyridyl-containing ligands, namely, 2,2′-bipyrimidine (bpm), 2,3-bis(2-pyridyl)pyrazine (dpp) and 2,3′-bis(2′-pyridyl)-5,6-dimethylquinoxaline (dpq), gave the new clusters: $[Os_4(\mu\text{-}H)_4(CO)_{10}(bpm)]$ **2**, $[Os_4(\mu\text{-}H)_4(CO)_{10}(dpp)]$ **3** and $[Os_4(\mu\text{-}H)_4(CO)_{10}(dpq)]$ **4**, respectively. The molecular structures of clusters **2**, **3** and **4** were established by X-ray diffraction analysis. Compound **3** underwent protonation to give the corresponding water soluble cationic cluster $[Os_4(\mu\text{-}H)_4(CO)_{10}(dppH)]^+$ **5** which has been characterized by positive-mode electrospray mass spectrometric analysis of the aqueous phase. Incorporation of compound **3** as a building block in the heterometallic supramolecular system has also been established.

Introduction

The reactions of pyridyl-containing ligands with various transition metal complexes are of considerable interest.[1–5] The interest is not only in the study of their spectroscopic, photophysical and photochemical properties, but also in the building of supramolecular structures using pyridyl-containing ligands as the spacer unit.[6–9] We have examined the reactions of trinuclear transition metal carbonyl clusters with some pyridyl-containing ligands and shown that novel functionalized pyridine containing clusters can be prepared.[10–12] In addition, we have reported the synthesis of some supramolecules of triosmium carbonyl clusters based on different pyridyl-containing spacers.[13–15]

In a recent paper, we described the reactions of the activated tetraosmium carbonyl cluster $[Os_4(\mu\text{-}H)_4(CO)_{10}(NCMe)_2]$[16] **1** with some pyridyl or phenanthroline type ligands and some fruitful results were obtained.[17] However, the related pyridyl-functionalized tetraosmium carbonyl clusters have not been well studied. It was believed that the pyridyl-functionalized tetraosmium carbonyl clusters can act as precursors for the building up of supramolecular species. In view of this, we have studied the reactions and reactivity of the activated tetraosmium carbonyl cluster with some pyridyl ligands such as 2,2′-bipyrimidine (bpm), 2,3-bis(2-pyridyl)pyrazine (dpp) and 2,3′-bis(2′-pyridyl)-5,6-dimethylquinoxaline (dpq).

In addition, we also report the electrospray mass spectrometry (ESI-MS) study of a protonated pyridyl-functionalized tetraosmium carbonyl cluster in an aqueous medium. Electrospray[18–20] is an ionization method which can efficiently desorb ions formed in solution into the gas phase for mass analysis. Nicholson and co-workers have reported that electrospray mass spectrometry can be applied to the analysis of some neutral triosmium carbonyl clusters, based[21] on ionization with Ag^+ to produce a parent ion of $[M + Ag]^+$. ESI-MS techniques have also been used to study the triosmium carbonyl cluster in the presence of alkoxide ion as an ionization agent in MeOH.[22] We herein report the synthesis of three new pyridyl-functionalized tetraosmium carbonyl clusters $[Os_4(\mu\text{-}H)_4(CO)_{10}L]$, (L = bpm, dpp and dpq) and the first electrospray mass spectrometric study of a protonated, cationic, pyridyl-functionalized tetraosmium carbonyl cluster in aqueous solution.

Results and discussion

Synthesis of $[Os_4(\mu\text{-}H)_4(CO)_{10}(bpm)]$ 2, $[Os_4(\mu\text{-}H)_4(CO)_{10}(dpp)]$ 3 and $[Os_4(\mu\text{-}H)_4(CO)_{10}(dpq)]$ 4

The activated tetraosmium carbonyl cluster **1** and one equivalent of 2,2′-bipyrimidine (bpm) were allowed to react in refluxing CH_2Cl_2 and a chelated cluster $[Os_4(\mu\text{-}H)_4(CO)_{10}(bpm)]$ **2** was obtained in moderate yield after TLC purification (Scheme 1). Cluster **2** has been fully characterized by conventional spectroscopic methods and the data are summarized in Table 1. The FAB mass spectrum of **2** shows an intense parent ion at *m*/*z* 1202. The room temperature ^1H NMR spectrum of **2** consists of a triplet at δ 7.61 and two multiplets at δ 9.19 and 9.35 which are attributed to the protons of the bpm ligand. The four very broad singlets in the negative region (δ −18.2, −18.6, −21.3 and −21.6) are due to the four metal hydrides on the tetraosmium core. This observation suggested some dynamic processes, related to hydride ligands, may be occurring at room temperature. An NMR spectrum has been recorded at a higher temperature (50 °C), however, the spectral features are essentially the same as the room temperature one. These four hydride signals turned into sharp singlets at −50 °C. This low temperature limit spectral feature is consistent with the ground-state structure of the cluster. This kind of dynamic behaviour involving hydrido ligand site-exchange is often observed in solution for organometallic transition metal cluster compounds.[23,24]

Cluster **1** and excess dpp or dpq were allowed to react under refluxing CH_2Cl_2 to give two chelated clusters $[Os_4(\mu\text{-}H)_4(CO)_{10}(dpp)]$ **3** and $[Os_4(\mu\text{-}H)_4(CO)_{10}(dpq)]$ **4**, in moderate yield, respectively. Both **3** and **4** were identified by solution spectroscopic methods (Table 1). The FAB mass spectra of **3** and **4** show a parent peak at *m*/*z* 1279 and 1357 respectively with the stepwise loss of terminal carbonyl ligands. The solution IR spectra of both **3** and **4** show a typical pattern within the carbonyl region for disubstituted Os_4 complexes. The ^1H

Table 1 Summary of spectroscopic data of clusters **2**–**7**

Cluster	IR (ν_{CO})[a] (cm^{-1})	^1H NMR[b] (δ, J/Hz)	FAB-MS[c]
2	2079s, 2048vs, 2019s, 1998s, 1975m	9.35 [m, 2H] 9.19 [m, 2H] 7.61 [t, J_{HH}, 5.3, 2H] −18.2 [s, 1H] −18.6 [s, 1H] −21.3 [s, 1H] −21.6 [s, 1H]	1202 (1202)
3	2079s, 2050vs, 2018s, 1998s, 1979m	9.24 [m, 2H] 8.69 [d, J_{HH} 8.4, 1H] 8.63 [d, J_{HH} 7.6, 1H] 8.07 [t, J_{HH} 7.8, 1H] 7.98 [d, J_{HH} 7.8, 1H] 7.66 [m, 1H] 7.58 [dd, J_{HH} 7.8, 7.6, 1H] 7.38 [m, 1H] 7.12 [d, J_{HH} 8.4, 1H] −18.1 [s, 1H] −18.8 [s, 1H] −21.0 [s, 1H] −21.6 [s, 1H]	1279 (1279)
4	2080s, 2048vs, 2020s, 1999s, 1975m	9.35 [d, J_{HH} 5.9, 1H] 8.60 [m, 1H] 7.96–8.08 [m, 1H] 7.68 [s, 2H] 7.47–7.38 [m, 2H] 7.32 [t, J_{HH} 5.9, 1H] 7.12 [m, 1H] 2.96 [s, 3H] 2.57 [s, 3H] −18.3 [s, 1H] −18.9 [s, 1H] −21.2 [s, 1H] −21.7 [s, 1H]	1357 (1357)
5	2132s, 2097s, 2066vs, 2041s, 2019s	9.57 [m, 2H] 9.06 [m, 2H] 8.47 [m, 2H] 8.12 [m, 2H] 7.58 [m, 1H] 7.21 [m, 1H] −17.9 [s, 1H] −18.7 [s, 1H] −20.7 [s, 1H] −21.5 [s, 1H]	1280 (1280)
6	2079s, 2050vs, 2018vs, 1998s, 1984m	9.79 [d, J_{HH} 5.8, 1H] 9.61 [m, 1H] 9.51 [d, J_{HH} 8.6, 1H] 9.02 [d, J_{HH} 8.6, 1H] 8.87 [m, 1H] 8.59 [m, 1H] 8.16 [m, 1H] 8.06 [m, 1H] 7.84 [m, 3H] 7.64 [m, 3H] 7.48 [m, 2H] 7.40 [m, 2H] 7.26 [m, 1H] 7.13 [m, 1H] 6.87 [m, 1H] −18.0 [s, 1H] −18.7 [s, 1H] −20.1 [s, 1H] −20.9 [s, 1H]	1754 (1754)
7	2106w, 2077s, 2050s, 2040s, 2020vs, 1981s, 1960s		2131 (2130)

[a] In CH_2Cl_2. [b] In $CDCl_3$. [c] Simulated value in parentheses.

NMR spectrum of **3** shows four doublets at δ 7.12, 7.98, 8.63 and 8.69, two multiplets at δ 7.38 and δ 7.66, a triplet at δ 8.07 and a double doublet at δ 7.58. The four singlets in the negative region are attributed to the four metal hydrides on the Os_4 core. The proton NMR spectrum of **4** shows a similar pattern to **3**, with resonance signals due to the pyridyl and quinoxaline protons of 2,3′-bis(2′-pyridyl)-5,6-dimethylquinoxaline in the range of δ 7.12–9.35, where the methyl protons give two singlets at δ 2.57 and 2.96. All of the ligand signals in **3** and **4** are found to be in a more downfield region than those of the free ligands upon coordination to the electron deficient tetraosmium core. Similar to cluster **2**, both **3** and **4** give four broad singlets corresponding to the four hydrides on the tetraosmium core.

The molecular geometry of cluster **2** is illustrated in Fig. 1 and the selected bond parameters are summarized in Table 2. The structure of **2** consists of a bipyrimidine ligand chelated on

Table 2 Selected bond distances (Å) and angles (°) for cluster **2**

Os(1)–Os(2)	2.955(2)	Os(1)–Os(3)	2.955(2)
Os(1)–Os(4)	3.026(2)	Os(2)–Os(3)	2.800(2)
Os(2)–Os(4)	2.937(2)	Os(3)–Os(4)	2.825(2)
Os(1)–N(1)	2.13(3)	Os(1)–N(2)	2.12(3)
Os(2)–Os(1)–Os(3)	56.55(5)	Os(2)–Os(1)–Os(4)	58.80(5)
Os(3)–Os(1)–Os(4)	56.35(4)	Os(1)–Os(2)–Os(3)	61.72(5)
Os(1)–Os(2)–Os(4)	61.81(5)	Os(3)–Os(2)–Os(4)	58.94(5)
Os(2)–Os(3)–Os(4)	62.95(5)	Os(1)–Os(3)–Os(4)	63.10(5)
Os(1)–Os(3)–Os(2)	61.73(5)	Os(1)–Os(4)–Os(2)	59.39(5)
Os(2)–Os(4)–Os(3)	58.11(5)	Os(1)–Os(4)–Os(3)	60.55(4)

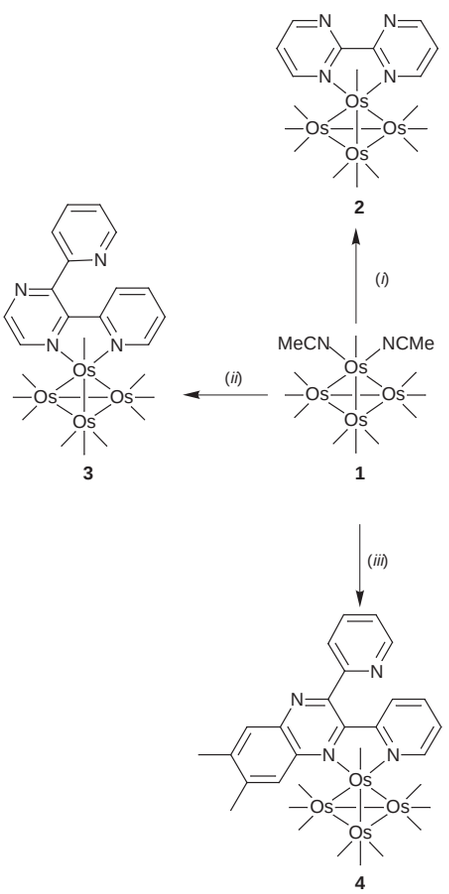

Scheme 1 (*i*) bpm, CH_2Cl_2, 2 h reflux; (*ii*) dpp, CH_2Cl_2, 2 h reflux; (*iii*) dpq, CH_2Cl_2, 2 h reflux.

one vertex [Os(1)] of the tetraosmium core. Each osmium atom, except Os(1) in the tetraosmium core, has three terminal carbonyl ligands. The Os(1)–N(1) and Os(1)–N(2) bond lengths [2.13(3) and 2.12(3) Å, respectively] in **2** are similar to those observed in the bipyridine substituted tetraosmium cluster [2.11(2) and 2.09(2) Å].[17] In the tetraosmium core, it is found that the Os(2)–Os(3) and Os(3)–Os(4) bonds [2.800(2) and 2.825(2) Å, respectively] are shorter than other Os–Os bonds with bridging hydrides in the molecule.

The molecular geometries of **3** and **4** are very similar in that the vertex of the tetraosmium core [Os(1)] is chelated by the ligand giving a disubstituted cluster in each case. Perspective drawings of **3** and **4** are shown in Figs. 2 and 3, respectively; and the selected bond lengths and angles are summarized in Tables 3 and 4. It is found that the pyridyl [N(1)–C(11)–C(12)–C(13)–C(14)–C(15)] and pyrazine [N(2)–C(16)–C(17)–N(3)–C(18)–C(19)] groups are bonded to Os(1) in a manner similar to that of $[Os_4(\mu\text{-}H)_4(CO)_{10}(2,2'\text{-bpm})]$ in cluster **2**. However, the molecular structure of **3** shows that these two rings ([N(1)–C(11)–C(12)–C(13)–C(14)–C(15), and N(2)–C(16)–C(17)–C(18)–C(19)]) are not co-planar and form a dihedral angle of

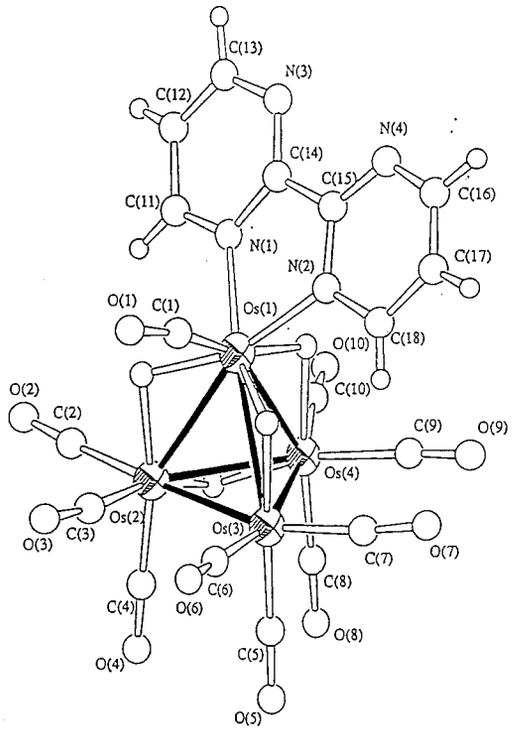

Fig. 1 A perspective drawing of $[Os_4(\mu\text{-}H)_4(CO)_{10}(bpm)]$ **2**.

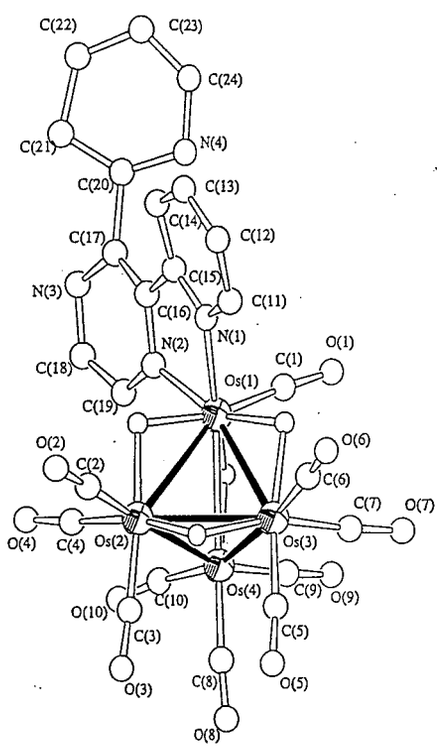

Fig. 2 A perspective drawing of $[Os_4(\mu\text{-}H)_4(CO)_{10}(dpp)]$ **3**.

16.7°. Another pyridyl ring [N(4)–C(20)–C(21)–C(22)–C(23)–C(24)] makes a larger dihedral angle [43.7°] with the pyrazine ring [N(2)–C(16)–C(17)–N(3)–C(18)–C(19)]. In the solid state, atoms N(3) and N(4) display an *anti* geometry which is probably due to the smaller steric repulsion between C(14) and the hydrogen associated with N(4).

The molecular structure of **4** is very similar to that of **3**, but the dihedral angle between the two rings N(1)–C(11)–C(12)–C(13)–C(14)–C(15) and N(2)–C(16)–C(17)–N(4)–C(19)–C(23)–C(22)–C(21)–C(20)–C(18) is 27.4°, and the Os–N bond in **3** [Os(1)–N(1): 2.07(3) Å] is a little bit shorter than that in **4**

Table 3 Selected bond distances (Å) and angles (°) for cluster **3**

Os(1)–Os(2)	3.004(2)	Os(1)–Os(3)	2.971(2)
Os(1)–Os(4)	2.932(2)	Os(2)–Os(3)	2.929(2)
Os(2)–Os(4)	2.823(2)	Os(3)–Os(4)	2.790(2)
Os(1)–N(1)	2.07(3)	Os(1)–N(2)	2.08(3)
Os(2)–Os(1)–Os(3)	58.71(5)	Os(2)–Os(1)–Os(4)	56.78(5)
Os(3)–Os(1)–Os(4)	56.42(5)	Os(1)–Os(2)–Os(3)	60.07(5)
Os(1)–Os(2)–Os(4)	60.32(6)	Os(3)–Os(2)–Os(4)	58.00(6)
Os(1)–Os(3)–Os(2)	61.22(5)	Os(1)–Os(3)–Os(4)	61.10(5)
Os(2)–Os(3)–Os(4)	59.10(6)	Os(1)–Os(4)–Os(2)	62.90(6)
Os(1)–Os(4)–Os(3)	62.49(5)	Os(2)–Os(4)–Os(3)	62.90(6)

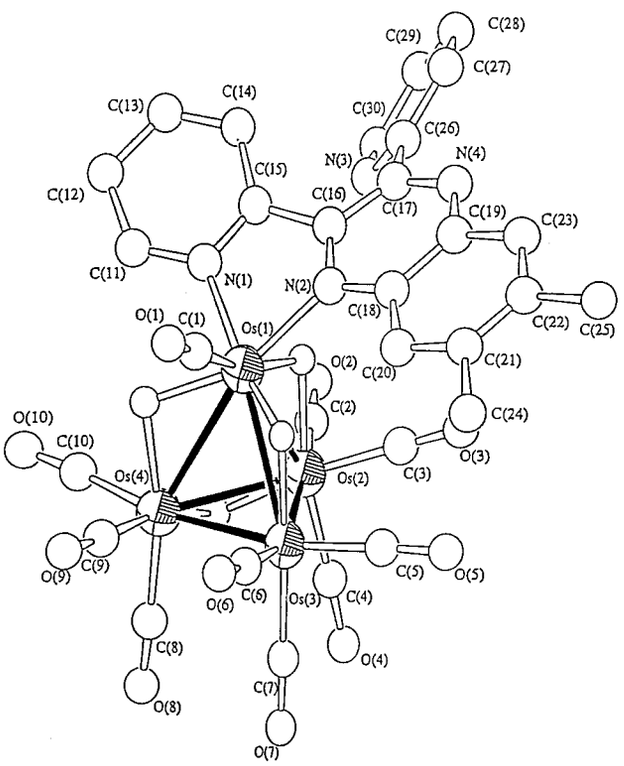

Fig. 3 A perspective drawing of $[Os_4(\mu\text{-}H)_4(CO)_{10}(dpq)]$ **4**.

[Os(1)–N(2): 2.12(2) Å] which may be due to the bulky dimethylquinoxaline group in **4**.

Reactivity study of $[Os_4(\mu\text{-}H)_4(CO)_{10}(dpp)]$ 3

Protonation of **3** by the addition of trifluoroacetic acid, CF_3CO_2H in CH_2Cl_2, results in a rapid change in colour from deep violet to light pink. Formation of a monocationic cluster **5** $[Os_4(\mu\text{-}H)_4(CO)_{10}(dppH)]^+$ was implied based on a shift of approximately 50 cm^{-1} for ν_{CO} to the high-energy region in the IR spectrum of **5** as compared to that in **3**. The ^1H NMR spectrum of **5** shows a similar set of resonances corresponding to the ligand protons. However, the proton signal arising from the pyridinium N-H moiety is not observed, probably due to the broadening effect obtained *via* coupling to the quadrupolar nitrogen atom.[25]

Low flow electrospray mass spectrometric study (ESI-MS) of the cationic cluster 5

Cationic cluster **5** was studied by the electrospray mass spectroscopic technique with water/methanol as the mobile phase. Cluster **5** showed a reasonable solubility in water and a drop of acetic acid was added to the sample solution to enhance the conductivity. The spectrum showed a clear parent peak at *m*/*z* 1280.7, Fig. 4(a). The soft ionization mode in ESI-MS reduces the degree of fragmentation as compared with other common ionization methods (*e.g.* EI or FAB), which can maximize the population of target species to enter the ion trap. One of the advantages of using the ion trap technique in mass spectrometric study is its good selectivity, unlike some sector or quadrupole MS, which enables the isolation of a particular target ion for further study by ejecting the other ions. A tandem mass spectroscopic study was carried out on **5** at *m*/*z* 1280 by ramping the amplitude of the radio-frequency (RF) across the ring electrode and the two endcaps. Such ramping of the RF induced fragmentation of ions in the ion trap. Fig. 4(b) shows the loss of two carbonyl ligands from **5** for a collision energy of 1 V, this agrees with the data for the full scan spectrum of **5**.

Table 4 Selected bond distances (Å) and angles (°) for cluster **4**

Os(1)–Os(2)	3.006(1)	Os(1)–Os(3)	2.966(2)
Os(1)–Os(4)	2.970(2)	Os(2)–Os(3)	2.815(2)
Os(2)–Os(4)	2.960(2)	Os(3)–Os(4)	2.789(1)
Os(1)–N(2)	2.12(2)	Os(1)–N(1)	2.08(2)
Os(2)–Os(1)–Os(3)	56.24(4)	Os(2)–Os(1)–Os(4)	59.37(4)
Os(3)–Os(1)–Os(4)	56.04(4)	Os(1)–Os(2)–Os(3)	61.16(3)
Os(1)–Os(2)–Os(4)	59.71(4)	Os(3)–Os(2)–Os(4)	57.69(4)
Os(1)–Os(3)–Os(2)	62.59(4)	Os(1)–Os(3)–Os(4)	62.05(4)
Os(2)–Os(3)–Os(4)	63.76(4)	Os(1)–Os(4)–Os(2)	60.92(3)
Os(1)–Os(4)–Os(3)	61.91(4)	Os(2)–Os(4)–Os(3)	58.55(4)

Supramolecule construction *via* $[Os_4(\mu\text{-}H)_4(CO)_{10}(dpp)]$ 3 as a precursor

Cluster **3** was allowed to react with 1 equivalent of $[Ru(\eta^2\text{-}OC_{10}H_6NO)_2(CO)(NCMe)]$ or $[Os_3(CO)_{10}(NCMe)_2]$ in refluxing $CHCl_3$ to give a purple compound $[Os_4(\mu\text{-}H)_4(CO)_{10}(dpp)\text{-}Ru(\eta^2\text{-}OC_{10}H_6NO)_2(CO)]$ **6** and a blue compound $[Os_4(\mu\text{-}H)_4(CO)_{10}(dpp)Os_3(\mu\text{-}H)(CO)_{10}]$ **7**, respectively (Scheme 2). The solution IR spectrum of **6** shows a similar ν_{CO} pattern to that in **3**. The ^1H NMR spectrum of **6** contains resonance signals due to the protons in **3** and the Ru complex. However, a satisfactory ^1H NMR spectrum of **7** could not be obtained due to solubility problems. The FAB mass spectra of **6** and **7** show an intense parent peak at *m*/*z* 1754 and 2131, respectively (Table 1). Both of the mass spectra show a daughter ion fragment envelope at 1279, which is attributed to **3**. There was excellent agreement between the calculated experimental isotope patterns for clusters **6** and **7**. Attempts to obtain single crystals of **6** and **7** for X-ray diffraction experiments have been unsuccessful so far. A modelling study on the structure of **3** shows that the pendant N(4) should be less reactive than N(3) due to blocking from the ring [N(1)–C(11)–C(12)–C(13)–C(14)–C(15)] which limits the accessibility of N(4). Therefore, we believe that the co-ordination of the dpp ligand in **6** and **7** is *via* pyrazine nitrogen rather than the pendant pyridine ring.

Experimental

None of the compounds reported here are particularly air-sensitive. However, all reactions and manipulations were carried out under Ar with the use of standard inert-atmosphere Schlenk techniques. The reactions were monitored by solution IR spectroscopy in the carbonyl stretching region. Solvents were dried by standard procedures and freshly distilled prior to use.[26] The ^1H NMR spectra were recorded on a Bruker DPX 300 spectrometer. Fast atom bombardment (FAB) mass spectra were obtained on a Finnigan MAT 95 mass spectrometer using a caesium source. The electrospray mass spectrometric study was carried out on a Finnigan LCQ™ quadrupole ion trap mass spectrometer.

All chemicals, except where stated, were purchased from commercial sources and used as received without any further purification. The starting cluster $[Os_4(\mu\text{-}H)_4(CO)_{10}(NCMe)_2]$ **1**

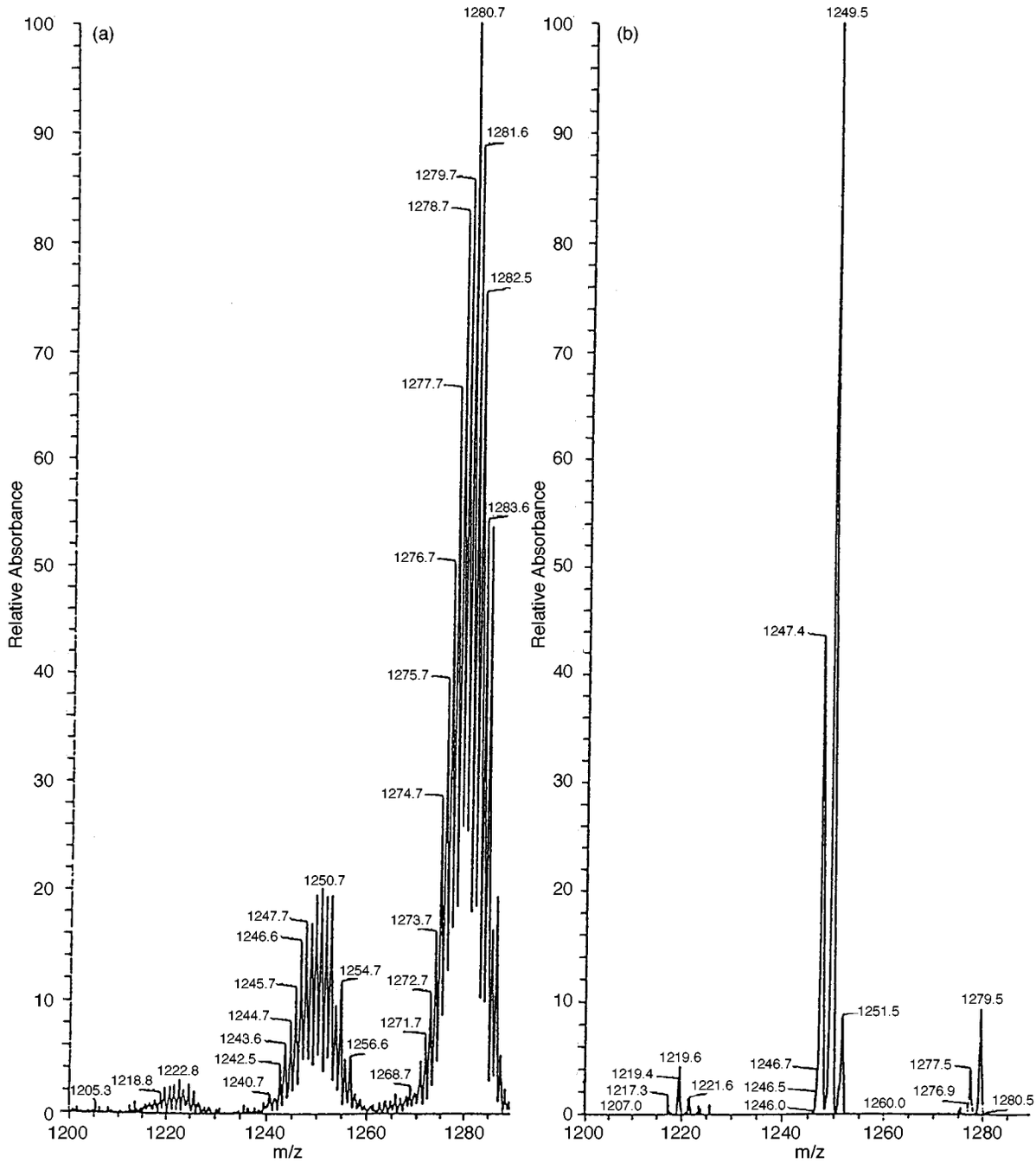

Fig. 4 (a) Electrospray mass spectrum of **5**. (b) Tandem mass spectrum of **5** at 20% of 5 V collision energy.

was prepared from $[Os_4(\mu\text{-}H)_4(CO)_{12}]$ following a slight modification of the literature methods,[27,28] and the mononuclear ruthenium carbonyl complex $[Ru(\eta^2\text{-}OC_{10}H_6NO)_2(CO)(NCMe)]$ was obtained and used according to the published method.[29] Routine separation of products, unless stated, was performed in air by thin-layer chromatography using plates coated with Merck Kieselgel 60 GF_{254}.

Preparation of $[Os_4(\mu\text{-}H)_4(CO)_{10}(bpm)]$ 2

Two equivalents of 2,2′-bipyrimidine (bpm) (32 mg, 0.2 mmol) and cluster **1** (113 mg, 0.1 mmol) were heated to reflux in CH_2Cl_2 under an argon atmosphere for 2 h. The solvent was removed under reduced pressure. The residue was purified by TLC using *n*-hexane/dichloromethane (1 : 1, v/v) as eluent. An intense brown band of **2** was obtained ($R_f = 0.3$) in 35% yield (42 mg). (Found: C, 18.05; H, 0.89; N, 4.70%. Calc. for $Os_4C_{18}H_{10}N_4O_{10}$: C, 17.97; H, 0.83; N, 4.66%).

Preparation of $[Os_4(\mu\text{-}H)_4(CO)_{10}(dpp)]$ 3 and $[Os_4(\mu\text{-}H)_4(CO)_{10}(dpq)]$ 4

A 3-fold excess of 2,3-bis(2-pyridyl)pyrazine (dpp) (70 mg, 0.3 mmol) or 2,3′-bis(2′-pyridyl)-5,6-dimethylquinoxaline (dpq) (93 mg, 0.3 mmol) and cluster **1** (113 mg, 0.1 mmol) were allowed to react in refluxing CH_2Cl_2 for 2 h and 3 h, respectively, until no further change was observed in the carbonyl stretching region in the solution IR spectra. The solvent was removed under reduced pressure and the residue was chromatographed on silica plate with *n*-hexane/dichloromethane (3 : 7, v/v for **3** and **4**) as eluent. Cluster **3** was isolated as a violet solid ($R_f = 0.4$) in 40% yield (51 mg), (Found: C, 22.51; H, 1.15; N, 4.32%. Calc. for $Os_4C_{24}H_{14}N_4O_{10}$: C, 22.54; H, 1.09; N, 4.38%) and cluster **4** was isolated as a deep violet solid ($R_f = 0.3$) in 25% yield (34 mg). (Found: C, 26.72; H, 1.53; N, 4.35%. Calc. for $Os_4C_{30}H_{20}N_4O_{10}$: C, 26.55; H, 1.47; N, 4.13%).

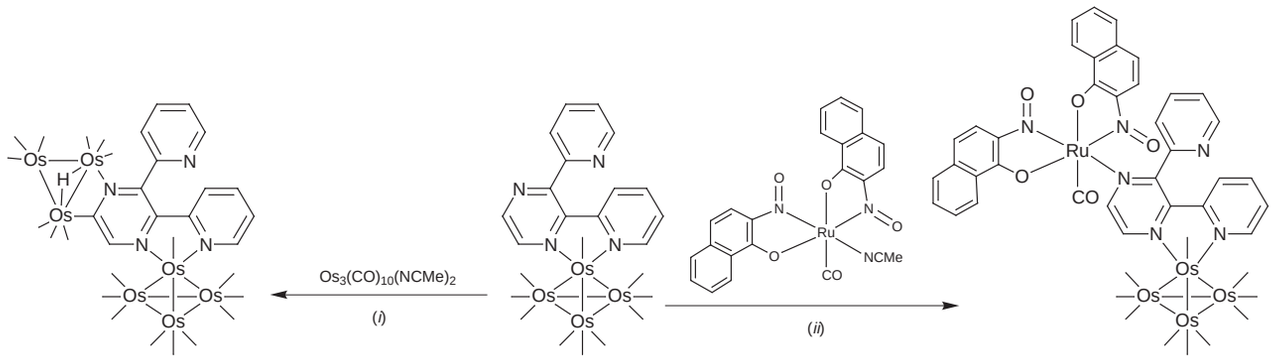

Scheme 2 (*i*) $CHCl_3$, 3 h reflux; (*ii*) CH_2Cl_2, 2 h reflux.

Protonation of $[Os_4(\mu\text{-}H)_4(CO)_{10}(dpp)]$ 3

$[Os_4(\mu\text{-}H)_4(CO)_{10}(dpp)]$ **3** (50 mg, 0.04 mmol) was dissolved in CH_2Cl_2 to give a violet solution. Trifluoroacetic acid, CF_3COOH, was added dropwise *via* an oven-dried syringe. The solution became light pink in colour. Positive electrospray spectrometric analysis revealed the presence of $[Os_4(\mu\text{-}H)_4(CO)_{10}(dpp)(H)]^+$ **5**.

Reaction of $[Os_4(\mu\text{-}H)_4(CO)_{10}(dpp)]$ 3 with $[Ru(\eta^2\text{-}OC_{10}H_6NO)_2(CO)(NCMe)]$

$[Os_4(\mu\text{-}H)_4(CO)_{10}(dpp)]$ **3** (100 mg, 0.08 mmol) and a 1.5-fold excess of $[Ru(\eta^2\text{-}OC_{10}H_6NO)_2(CO)(NCMe)]$ (62 mg, 0.16 mmol) were heated to reflux in $CHCl_3$ for 3 h. The solvent was removed and the residue was chromatographed on silica plate with *n*-hexane/dichloromethane (1:1, v/v) as eluent. A deep violet cluster $[Os_4(\mu\text{-}H)_4(CO)_{10}(dpp)Ru(\eta^2\text{-}OC_{10}H_6NO)_2(CO)]$ **6**, was isolated ($R_f = 0.4$) in 10% yield (14 mg).

Reaction of $[Os_4(\mu\text{-}H)_4(CO)_{10}(dpp)]$ 3 with $[Os_3(CO)_{10}(NCMe)_2]$

$[Os_4(\mu\text{-}H)_4(CO)_{10}(dpp)]$ **3** (100 mg, 0.08 mmol) and $[Os_3(CO)_{10}(NCMe)_2]$ (75 mg, 0.08 mmol) were allowed to reflux for 2 h. The solvent was removed under reduced pressure. The residue was purified by TLC using *n*-hexane/dichloromethane (1:1, v/v) as eluent. A blue cluster $[Os_4(\mu\text{-}H)_4(CO)_{10}(dpp)Os_3(\mu\text{-}H)(CO)_{10}]$ **7** was obtained ($R_f = 0.3$) in 10% yield (15 mg).

Molecular modelling

Molecular modelling was carried out on a CAChe Tektronix computer using the MM2 parameter. The energy terms for the interactions included: bond stretch, bond angle, dihedral angle, improper torsion, van der Waals, electrostatics and hydrogen bond.

Calculations have been performed on **3** and **3′**, where **3′** is essentially the same as **3** except that there is a rotation of 180° on the C(17)–C(20) bond so as to position both N(3) and N(4) on the same side (Fig. 2). The average total energies of **3** and **3′** are 7661 kJ mol^{-1} and 8166 kJ mol^{-1}, respectively.

Low flow electrospray mass spectrometric study (ESI-MS) of $[Os_4(\mu\text{-}H)_4(CO)_{10}(dpp)(H)]^+$ 5

The electrospray mass spectrum of the cationic cluster **5** was obtained in the positive ion mode using deionized water/methanol (v/v, 95:5) as the mobile phase. Dilution of the complex was carried out in deionized water (*ca.* 2 cm^3). The sample was injected *via* a 250 μl microliter syringe at the rate of 3 μl min^{-1}, whereas the sheath liquid was injected by a 500 μl microliter syringe with a doubled sample injection rate. A drop of acetic acid was added to enhance the spray current. The spray voltage of the ESI source was set at 4 kV. Every analytical scan at full scan and MS^2 consisted of 3 microscans and 5 microscans, respectively. The ion injection time for the ion trap in full-scan and MS^2 was 11 ms and 48 ms, respectively, where the multiplier for both studies was set at −930 V. Nitrogen gas was employed as the sheath gas and auxiliary gas for nebulising and spray enhancement purposes. The heated capillary temperature was set at 180 °C due to the high boiling point of water compared with other common solvents. The tube gate offset was set at −15 V in order to optimize the intensity of the parent peak.

X-Ray crystallography

Crystals of **2**, **3** and **4** suitable for X-ray analysis were obtained from slow evaporation of their CH_2Cl_2/hexane mixture (**2**, **3**) and CH_2Cl_2/benzene mixture (**4**) at room temperature over a period of 3 days. All pertinent crystallographic data and other experimental details are summarized in Table 5. Intensity data were collected at ambient temperature on a Rigaku AFC7R (**3**) or a MAR research image plate scanner (**2** and **4**) using Mo-Kα radiation ($\lambda = 0.71073$ Å) with a graphite-crystal monochromator. The ω–2θ scan technique with a scan rate of 16° min^{-1} (in ω) was used for **3**, whereas the ω scan technique was employed for **2** and **4** and 60 × 3°, frames with 5 minutes per frame were used. The intensity data were corrected for Lorentz and polarization effects. The ψ-scan method[30] was used for the absorption correction for **3**. However, an approximation to absorption correction by inter-image scaling was made for the other structures. The structures were solved by a combination of direct methods; (SHELXS86)[31] for **2**, (SIR92)[32] for **3** and (SIR88)[33] for **4**; and difference Fourier techniques. The structures were refined by full-matrix least squares analysis on *F*, with Os atoms refined anisotropically and other non-hydrogen atoms isotropically. The hydrogen atoms of the organic moieties were generated in their idealized positions (C–H, 0.95 Å), while hydride atom positions were estimated by potential energy minimizations.[34] All hydrogen atoms were included in the structure factor calculations but were not refined. There are potential ambiguities in the assignment of N(4) and C(21) for complex **3** and N(3) and C(27) for complex **4**. In both structures, we have exchanged the positions of nitrogen and carbon and carried out the refinement. The reported models gave slightly smaller *R*-factors, but more importantly the thermal factors associated with N(4)/C(21) for **3**, and N(3)/C(27) for **4** are more reasonable. In structure **4**, a positional disorder for benzene solvate was encountered. They were refined as a rigid group. All calculations were performed on a Silicon Graphics workstation using the program package TeXsan.[35]

CCDC reference number 186/1274.

Acknowledgements

W. T. W. acknowledges financial support from the Hong Kong Research Grants Council and The University of Hong Kong.

Table 5 Crystallographic data, data collection and structure solution parameters for clusters **2**–**4**

	2	**3**	**4**
Empirical formula	$Os_4N_4O_{10}C_{18}H_{10}$	$Os_4N_4O_{10}C_{24}H_{14}$	$Os_4N_4O_{10}C_{30}H_{20}\cdot 2C_6H_6$
M	1203.1	1279.2	1513.54
Crystal colour, habit	Red, block	Dark, plate	Red, block
Crystal size/mm	0.12 × 0.18 × 0.21	0.12 × 0.32 × 0.32	0.21 × 0.22 × 0.29
Crystal system	Monoclinic	Triclinic	Triclinic
Space group	$C2/c$ (no. 15)	$P\bar{1}$ (no. 2)	$P\bar{1}$ (no. 2)
a/Å	31.627(2)	13.706(3)	11.590(1)
b/Å	8.503(1)	15.443(3)	12.774(1)
c/Å	22.832(2)	8.613(2)	17.110(1)
α/°	90	101.72(2)	93.11(1)
β/°	127.01(2)	90.26(2)	96.49(1)
γ/°	90	112.45(1)	111.82(2)
U/Å^3	4902(1)	1643.0(7)	2323.8(5)
Z	8	2	2
D_c/g cm^{-3}	3.260	2.586	2.163
$F(000)$	4240	1140	1392
μ(Mo-Kα)/cm^{-1}	207.13	154.61	109.50
$T_{max,min}$	—	1.00, 0.472	—
Diffractometer	MAR Research Image Plate Scanner	Rigaku AFC7R	MAR Research Image Plate Scanner
2θ max collected/°	51.2	45.0	51.1
No. reflections collected	22437	4519	12112
No. unique reflections	7123	4301	5931
No. observed reflections [$I > 3\sigma(I)$]	1842	1913	2990
R^a	0.051	0.048	0.050
R'^b	0.064	0.053	0.059
Goodness of fit	1.49	1.55	1.40
Residual electron density/e Å^{-3}	1.67 to −2.34	1.97 to −2.16	1.11 to −1.56

^{a} $R = \Sigma||F_o| - |F_c||/|F_o|$. ^{b} $R' = [\Sigma w(|F_o| - |F_c|)^2/\Sigma wF_o^2]^{\frac{1}{2}}$ where $w = 1/[\sigma^2(F_o)] = [\sigma_c^2(F_o) + (p^2/4)(F_o)^2]^{-1}$.

Y. Y. C. acknowledges the receipt of a postgraduate studentship, the Hung Hing Ying Scholarship and the Michael Gale Scholarship administered by The University of Hong Kong and The Hong Kong Telecom Foundation, respectively. We also thank Dr H. L. Kwong of the City University of Hong Kong for his experimental assistance in the preparation of $[Os_4(\mu\text{-}H)_4(CO)_{12}]$; and Mr. Xiaolin Zheng of Finnigan MAT for his advice on electrospray mass spectrometry.

References

1 T. S. Akasheh, I. Jibril and A. M. Shraim, *Inorg. Chim. Acta*, 1990, **175**, 171.
2 E. Amouyal and A. Himsi, *J. Chem. Soc.*, *Dalton Trans.*, 1990, 1841.
3 J. W. M. van Oustersterp, D. J. Stufkens, J. Fraanje, K. Goubiyz and A. Vlcek, *Inorg. Chem.*, 1995, **34**, 4756.
4 E. Z. Jandrasics and F. R. Keene, *J. Chem. Soc.*, *Dalton Trans.*, 1997, 153.
5 A. M. W. C. Thompson, M. C. C. Smailes, J. C. Jeffery and M. D. Ward, *J. Chem. Soc.*, *Dalton Trans.*, 1997, 737.
6 R. G. Brewer, G. E. Jensen and K. Brewer, *Inorg. Chem.*, 1994, **33**, 124.
7 D. A. Bardwell, F. Barigelletti, R. L. Cleary, L. Flamigni, M. Guardgli, J. C. Jeffery and M. D. Ward, *Inorg. Chem.*, 1995, **34**, 2438.
8 A. Neels, B. M. Neels, H. Stoeckli-Evans, A. Clearfield and D. M. Poojary, *Inorg. Chem.*, 1997, **36**, 3402.
9 E. C. Constable, R. Martinez-Máñez, A. M. W. C. Thompson and J. V. Walker, *J. Chem. Soc.*, *Dalton Trans.*, 1994, 1585.
10 W. Y. Wong and W. T. Wong, *J. Chem. Soc.*, *Dalton Trans.*, 1995, 3995.
11 W. Y. Wong and W. T. Wong, *J. Chem. Soc.*, *Dalton Trans.*, 1995, 1497.
12 W. Y. Wong and W. T. Wong, *J. Chem. Soc.*, *Dalton Trans.*, 1996, 1853.
13 W. Y. Wong, W. T. Wong and K. K. Cheung, *J. Chem. Soc.*, *Dalton Trans.*, 1995, 1379.
14 W. Y. Wong and W. T. Wong, *J. Chem. Soc.*, *Dalton Trans.*, 1996, 1853.
15 W. Y. Wong and W. T. Wong, *J. Chem. Soc.*, *Dalton Trans.*, 1996, 3209.
16 Y. Y. Choi and W. T. Wong, *J. Organomet. Chem.*, 1996, **542**, 121.
17 Y. Y. Choi and W. T. Wong, *J. Organomet. Chem.*, in the press.
18 C. M. Whitehouse, R. N. Dreyes, M. Yamashita and J. B. Fenn, *Anal. Chem.*, 1985, **57**, 675.
19 S. J. Gaskell, *J. Mass Spectrom.*, 1997, **32**, 677.
20 J. B. Fenn, M. Mann, C. K. Mong, S. F. Wong and C. M. Whitehouse, *Mass Spectrom. Rev.*, 1990, **9**, 37.
21 W. Henderson and B. K. Nicholson, *J. Chem. Soc.*, *Dalton Trans*, 1998, 519.
22 W. Henderson, J. S. McIndoe, B. K. Nicholson and P. J. Dyson, *Chem. Commun.*, 1996, 1183.
23 M. R. Churchill and R. A. Lashewycz, *J. Am. Chem. Soc.*, 1977, **99**, 7384.
24 M. R. Churchill, R. A. Lashewycz, J. R. Shapley and S. I. Richter, *Inorg. Chem.*, 1980, **19**, 1277.
25 C. P. Gibson and L. F. Dahl, *Organometallics*, 1988, **7**, 543.
26 D. D. Perrin and W. L. F. Armarego, *Purification of Laboratory Chemicals*, 4th ed, Pergamon, Oxford, 1996.
27 H. D. Kaesz, S. A. R. Knox, J. W. Koepke and R. B. Saillant, *J. Chem. Soc.*, *Chem. Commun.*, 1971, 477.
28 C. Zuccaro, G. Pampaloni and F. Calderazzo, *Inorg. Synth.*, 1989, **26**, 169.
29 K. K. H. Lee and W. T. Wong, *J. Organomet. Chem.*, 1997, **547**, 329.
30 A. C. T. North, D. C. Phillips and F. S Mathews, *Acta Crystallogr.*, *Sect. A*, 1968, **24**, 351.
31 G. M. Sheldrick, in *Crystallographic Computing 3*, ed. G. M. Sheldrick, C. Kruger and R. Goddard, Oxford University Press, Oxford, 1985, p. 175.
32 A. Altomare, M. C. Burla, M. Cascarano, C. Giacovazzo, A. Guagliardi and G. Polidori, *J. Appl. Crystallogr.*, 1994, **27**, 435.
33 M. C. Burla, M. Camalli, G. Cascarano, C. Giacovazzo, G. Polidori, R. Spagna and D. Viterbo, *J. Appl. Crystallogr.*, 1989, **22**, 389.
34 A. G. Orpen, *J. Chem. Soc.*, *Dalton Trans.*, 1980, 2509.
35 TeXsan: *Crystal Structure Analysis Package*, Molecular Structure Corp., Houston, TX, 1985 and 1992.

Paper 8/08124G